

# UNIVERSITY *of* York

This is a repository copy of *Micro cracks distribution and power degradation of polycrystalline solar cells wafer: Observations constructed from the analysis of 4000 samples.*

White Rose Research Online URL for this paper:  
<https://eprints.whiterose.ac.uk/177729/>

Version: Accepted Version

---

## Article:

Dhimish, Mahmoud (2020) Micro cracks distribution and power degradation of polycrystalline solar cells wafer: Observations constructed from the analysis of 4000 samples. *Renewable Energy*. pp. 466-477. ISSN 0960-1481

<https://doi.org/10.1016/j.renene.2019.06.057>

---

## Reuse

This article is distributed under the terms of the Creative Commons Attribution-NonCommercial-NoDerivs (CC BY-NC-ND) licence. This licence only allows you to download this work and share it with others as long as you credit the authors, but you can't change the article in any way or use it commercially. More information and the full terms of the licence here: <https://creativecommons.org/licenses/>

## Takedown

If you consider content in White Rose Research Online to be in breach of UK law, please notify us by emailing [eprints@whiterose.ac.uk](mailto:eprints@whiterose.ac.uk) including the URL of the record and the reason for the withdrawal request.

# Micro Cracks Distribution and Power Degradation of Polycrystalline Solar Cells Wafer: Observations Constructed from the Analysis of 4000 Samples

*Mahmoud Dhimish*

*University of Huddersfield, Co-Director of Photovoltaics Laboratory, Huddersfield HD1 3DH, United Kingdom*

**Abstract**—In this paper, the impact of Photovoltaic (PV) micro cracks is assessed through the analysis of 4000 polycrystalline silicon solar cells. The inspection of the cracks has been carried out using an electron microscopy, which facilitate the detection of the cracks though the acquisition of both Everhart-Thornley Detector (ETD) and the Back Scatted Electron Diffraction (BSED) image, where it was found that the size micro cracks are ranging from 50 $\mu$ m to a maximum of 4mm. Micro cracks have been categorized into two main categories, including cracks in the solar cell front or rear contact. Several remarkable observations have been found, including but not limited to, (i) the output power loss due to micro cracks varies from 0.9% to 42.8%, subject to micro crack type and size, (ii) cracks in solar cells fingers reduce the finger width, resulting an increase in the output power loss by at least 1.7%, and (iii) there is a substantial correlation between PV hot-spots and the presence of micro cracks, while minimum increase in the cell temperature is observed at 7.6 °C.

**Keywords**—Photovoltaic Micro Cracks; PV Defects; Hot-Spots; Output Power Loss; Micro Analysis; Electron Microscopy Imaging.

## I. Introduction

Nowadays the lifetime of photovoltaic (PV) modules is an important target for the sustainable development of PV technologies. According to the International Electro-Technical Commission (IEC) 61215 PV qualification standard [1], PV modules are subject to multiple failure modes, ultimately an increase of PV micro cracks [2-3] and PV hot-spotting phenomenon [4-5] have been widely acknowledged. For instance, limited approaches and examination of such faults have been raised, and therefore, further data inspection and validation of typical PV failure have to be assessed and analysed comprehensively.

In order to examine PV micro cracks several methods have been proposed, including but not limited to the Laser scanning technique [6], Electron Microscopy (EM) analysis [7], Photoluminescence (PL) imaging technique [8], and the widely used Electroluminescence (EL) method [9].

F. Haase et al. [10] found that PV micro cracks do not reduce the output power of affected solar cells by more than 2.5%, only if the crack does not harm the fingers or busbars. While, a real-time long-term data analysis of multiple cracked PV modules were analysed by M. Dhimish et al. [11]. It was observed that output power of cracked PV modules ranging from -0.5% to -19.7%; depending on the crack size, orientation and location.

35 Furthermore, the micro crack analysis on gallium arsenide (GaAs) PV solar cells has been carried out by S.  
36 Oh et al. [12]. It was observed that the crack density, defined as the total length of the micro crack per unit  
37 area, is found to be in the range from 13.8 to 33.2 cm<sup>-1</sup> in all investigated solar cell samples of 1620. On  
38 the other hand, the analysis of the output power loss and cracks distribution have not been considered.

39 PV micro cracks are major cause of hot-spotting. PV hot-spots are a reliability problem in PV modules; this  
40 phenomenon is distinguished when a mismatched/cracked solar cell heats up significantly and reduces the  
41 PV module output power [13-14]. PV hot-spots can be easily detected using infrared inspection, which  
42 nowadays has become a common practice in current PV fault diagnosis as presented in [15]. However, the  
43 correlation between micro cracks and hot-spotting has not widely been considered, while the largest up-to-  
44 date study on PV hot-spotting has been reported by our previous work [16]. Furthermore, PV hot-spots can  
45 cause a permanent loss in the output power of PV module, and could be reach up to -25% of the PV module  
46 maximum power point.

47 PV hot-spotting can be mitigated using various methods such as novel distributive maximum power point  
48 tracking (MPPT) method [17-18], adoption of bypass diodes which are parallelized with the PV modules  
49 [19], and most recently, a novel two MOSFET layer method developed by [20-21] improved the output  
50 power of hot-spotted PV modules by at least 8% under various environmental conditions.

51 The main contribution of this work is to present the impact of micro cracks; ranging from 50μm to a maximum  
52 of 4mm, on the output power performance of solar cells. A total of 4000 cracked samples has been examined.  
53 Various major findings have been observed, including:

- 54 1) The output power loss due to micro cracks ranging from 0.9 to 42.8%.
- 55 2) Cracks in solar cells fingers reduce the finger width, resulting an increase in the power loss.
- 56 3) There is a substantial correlation between the hot-spots and micro cracks, multiple results were observed  
57 by the reason of the heat expansion due to the micro cracks affect.

## 58 II. Methodology

### 59 A. Electron Microscopy

60 Nowadays in order to examine the micro cracks in the solar wafers, an electron microscopy shown in Fig.  
61 1 has been used. The microscopy is interfaced with a personal computer (PC) using a data acquisition board.  
62 The acquisition of both the Everhart-Thornley Detector (ETD) and the Back Scattered Electron Diffraction  
63 (BSED) is facilitated using the acquisition board as presented Fig. 1.

64 The BSED is a microstructural-crystallographic characterization technique normally use to study any  
65 crystalline or polycrystalline materials [22], whereas the ETD consists of a secondary electron and back-  
66 scattered electron detector, this detector is used to increase the efficiency of existing secondary electron  
67 detectors by adding a light pipe to carry the photon signal from the scintillator inside the evacuated  
68 specimen chamber of the electron microscopy [23]. In fact, it is not necessary to capture both images, but,  
69 for a better resolution and detection of the inspected wafer, both images have been captured.

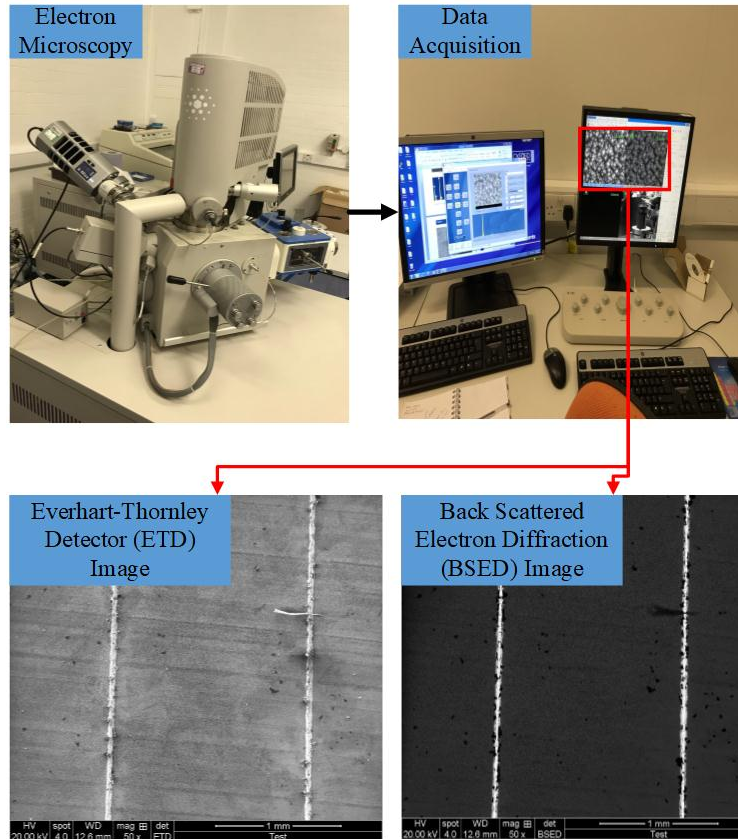


Fig. 1. Electron microscopy facility used to inspect the cracked solar cell samples. The microscope has a data acquisition system which facilitate the monitoring for both the ETD and BSED images using a personal computer

70 **B. Examined Solar Cell Samples**

71 In this article, the examination of 4000 cracked solar cell have been examined; example of multiple samples  
 72 are shown in Fig. 2(a); showing both front and rear view for diffident types of cracks. All tested samples  
 73 are dismantled from actual PV modules operated in a field across the UK. The solar cells have been on  
 74 actual operation for 5 to 13 years.

75 All main electrical parameters of the cracked samples have been tested under standard test conditions  
 76 (STC), where the solar irradiance is equal to 1000 W/m<sup>2</sup> and ambient temperature of 25 °C; main electrical  
 77 parameters are shown in Table 1.

78 Fig. 2(b) shows the location of the fingers and the solar cell busbar. Solar cell fingers are the metallic  
 79 rectangular–shape grid connectors which collect the generated current for devlry to the busbar. The busbar  
 80 is constructed from copper, coated with silver to enhance the current conductivity (front side) as well as to  
 81 lower oxidization (rear side).

Table 1 Examined solar cells main electrical parameters

Electrical Parameter	Theoretical Value – Taken form manufacturer data sheet
Voltage at maximum power point ( $V_{mpp}$ )	0.48 V
Open circuit voltage ( $V_{oc}$ )	0.61 V
Power at maximum power point ( $P_{mpp}$ )	3.10 W
Current at maximum power point ( $I_{mpp}$ )	6.46 A
Short circuit current ( $I_{sc}$ )	7.12 A

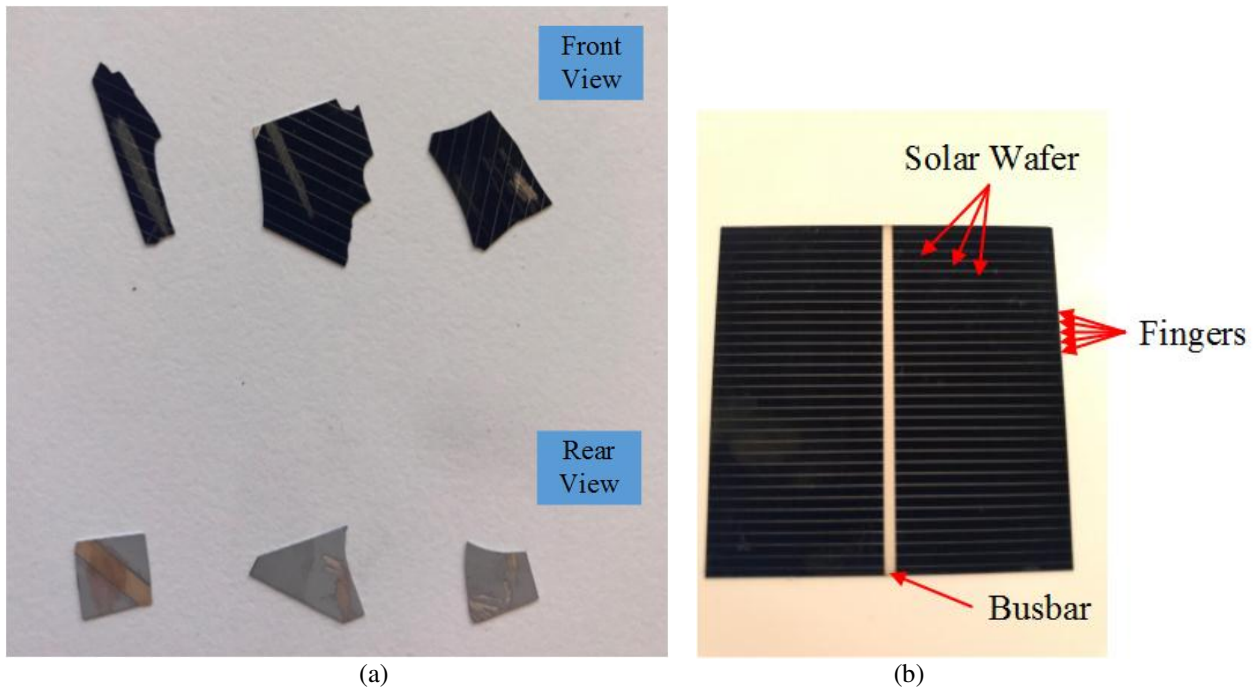


Fig. 2. (a) Example of the front and rear view for multiple examined solar cell wafers, (b) Solar cell wafer, fingers and busbar

### 82 C. Distribution and Data Collection Process

83 The examined solar cells samples have been distributed according to the existence of the micro crack type.  
 84 The analysis and data collection were distributed across front and rear view/side of the solar cell damage,  
 85 including:

#### 86 **Front View:**

- 87 1) Wafer + Fingers (Fig. 3(a)): micro cracks affecting both wafer and the fingers of the solar cell.
- 88 2) Wafer + Busbar (Fig. 3(b)): existence of micro cracks on solar cell wafer and busbar, but not
- 89 fingers.
- 90 3) Wafer + Fingers + Busbar (Fig. 3(c)): micro cracks affecting the wafer, fingers, and the busbars.

#### 91 **Rear Contact:**

- 92 1) Micro cracks affecting rear surface of the solar cell, example shown in Fig. 3(d).
- 93 2) Micro cracks affecting both rear surface of the solar cell and the rear busbar, example shown in
- 94 Fig. 3(e).

95 All observed micro cracks have a length ranging from  $50\mu\text{m}$  to a maximum of 4mm, therefore, the output  
 96 power analysis as well as the observations in the rest of the article are based on this assumption, and  
 97 ultimately, different crack length would result different observations.

98 The percentage of occurrence of the micro cracks in all tested samples are summarized as follows:

- 99 1) Wafer + Fingers presenting 39%; 1560 samples.
- 100 2) Wafer + Busbar presenting 17%; 680 samples.
- 101 3) Wafer + Fingers + Busbar presenting 36%; 1440 samples.
- 102 4) Rear surface presenting 6%; 240 samples.
- 103 5) Rear surface + Rear Busbar presenting 2%; 80 samples.

104 It is worth noting that the number of cracked busbars or fingers has not been considered in the data analysis.  
 105 There are two reasons behind this choice including, (i) the data collection and analysis of the output power  
 106 loss will fluctuate rapidly if the number of fingers and busbars are counted, and (ii) in order to draw relevant  
 107 conclusions with the consideration of multiple case studies, it would help to classify which micro crack  
 108 type/category has the most significant impact on the output power loss; resulting a generic/extensive gained  
 109 knowledge on the studied samples, where the outcomes can be used extensively across a number of other  
 110 studies, including PV degradation, PV manufacturing analysis and solar cell micro cracks detection  
 111 systems.

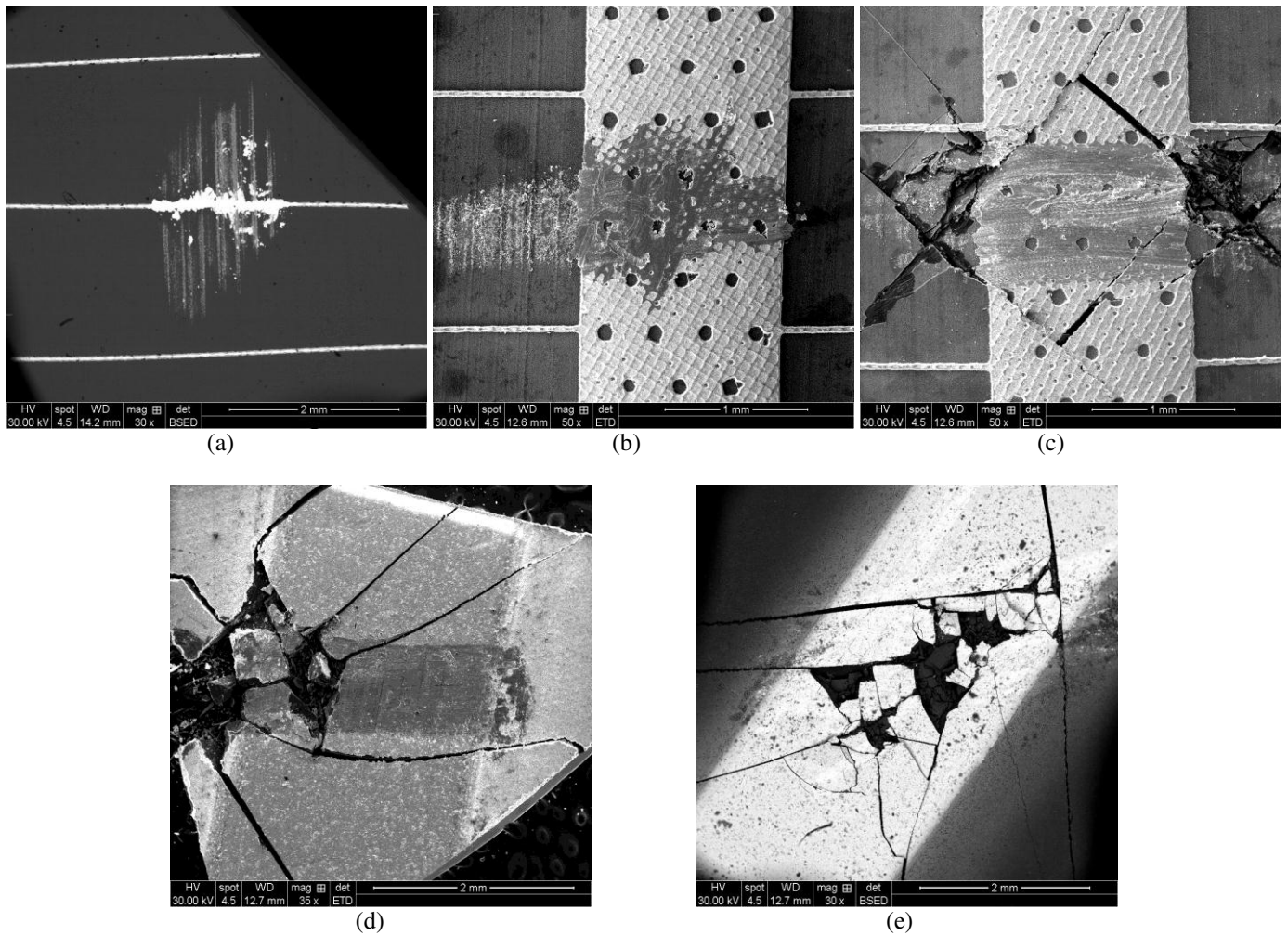


Fig. 3. Examples of the distribution for the micro cracks in different solar cell samples. (a) Micro cracks affecting solar cell wafer and fingers, (b) Micro cracks affecting solar cell wafer and busbars, (c) Micro cracks affecting solar cell wafer, fingers and busbar, (d) Micro cracks in the rear surface of the solar cell, (e) Micro cracks affecting rear surface of the solar cell as well as the rear busbar

### 112 III. Results

#### 113 A. Power Loss Analysis

114 In this section, the evaluation of the power loss of all examined PV solar cell is presented. The measured  
115 power loss of the solar cells is captured while experimentally illuminating the cells under standard test  
116 conditions (STC), where the solar irradiance is equal to 1000 W/m<sup>2</sup>, and cell surface temperature of 25 °C,  
117 the experimental setup is shown in Fig. 6(b). The output power loss is measured by the following formula:

$$118 \quad \text{Power Loss (\%)} = 100 - \left( \frac{P_{\text{Micro cracked solar cell}}}{P_{\text{Theoretical maximum power}}} \times 100 \right) \quad (1)$$

119 where  $P_{\text{Micro cracked solar cell}}$  is the actual measured output power of the tested micro cracked solar cell  
120 sample, whereas  $P_{\text{Theoretical maximum power}}$  is the theoretical power taken from the datasheet; the value  
121 for the theoretical power is equal to 3.1 W, presented earlier in Table 1.

122 According to Fig. 4(a), the solar cell samples affected by cracks in the front contact have a power loss  
123 ranging from:

- 124 1) Cracks in Wafer + Finger: -1.7% to -13.5%.
- 125 2) Cracks in Wafer + Busbar: -0.9% to -17.1%.
- 126 3) Cracks in Wafer + Finger + Busbar: -8.9% to -42.8%.

127 Evidently, the cracks affecting solar wafer, fingers and the busbar have the uppermost power loss, with  
128 mean of 25.52%, whereas the second maximum mean output power loss of 9.01% is obtained for the solar  
129 cells affected by micro cracks in the solar wafer and the busbar. The minimum output power loss is observed  
130 for solar cells that are affected by micro cracks across the wafer and fingers, their mean output power loss  
131 is equal to 7.59%.

132 According to the solar cell samples affected by rear contact micro cracks, it was observed that loss in the  
133 output power is very limited (mean of 1.48%) for the rear surface cracks, however, there are an increase in  
134 the output power loss due to the rear contact cracks affecting both surface and the rear busbar, where it was  
135 found that the mean output power loss is equal to 7.99%.

136 It is noticeable that front contact micro cracks have the most significant impact on the overall performance  
137 of the solar cells because these cracks affects the surface of the junction, ultimately limiting the amount of  
138 solar energy to be extracted by the cell. On the other hand, the output power loss for micro cracked rear  
139 surface is far less than the front contact, since it is much further away from the junction, whereas the rear  
140 busbar plays significant role in driving the solar cell current, therefore, cracks in rear and front busbar have  
141 a much higher output power loss.

142 There are a number of observations that have been identified using the studied sample set, including the  
143 correlation between micro cracks and hot-spots in the micro cracked solar cells. These observations are  
144 discussed in the following sections.

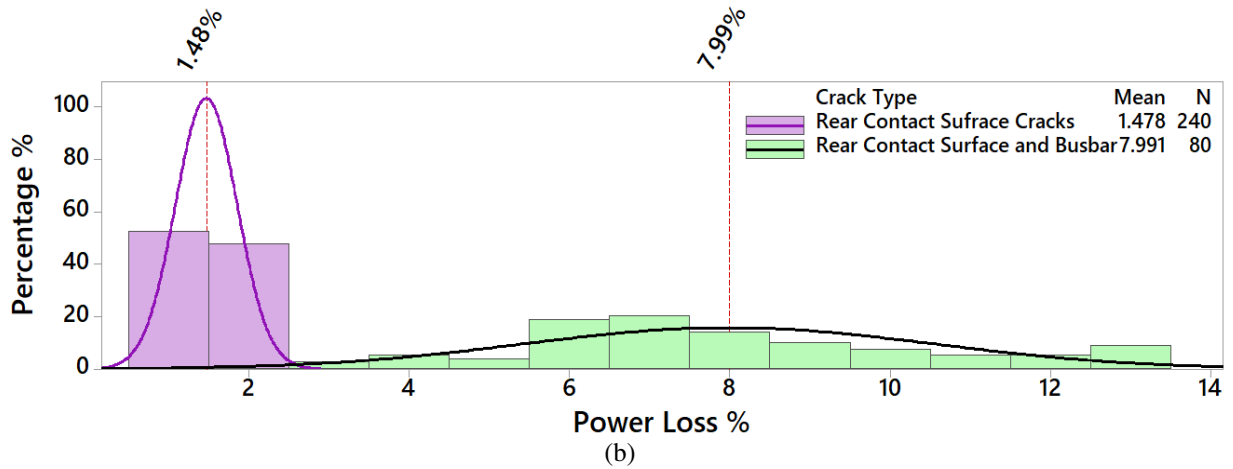
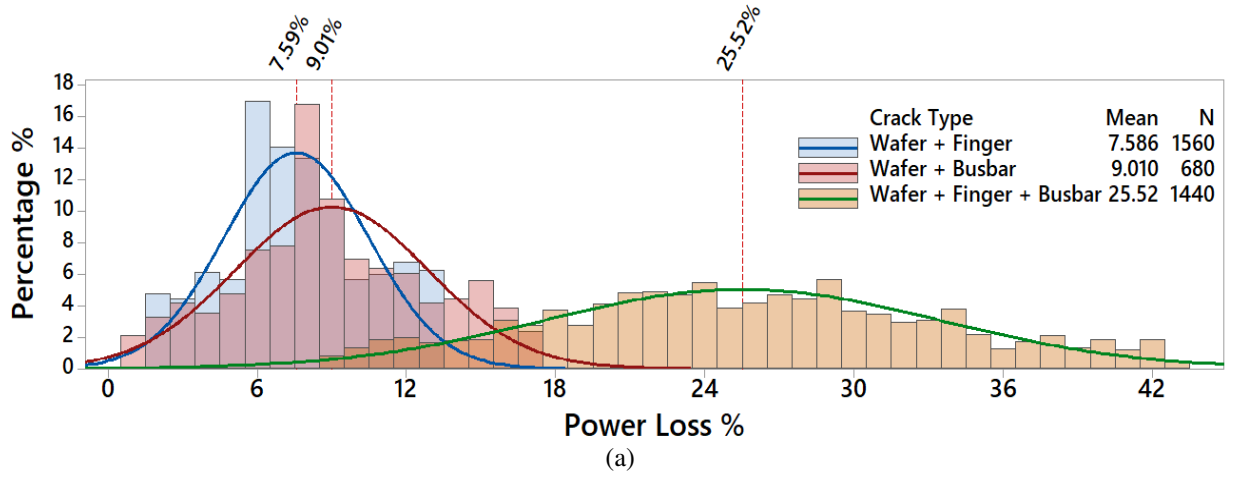


Fig. 4. Power loss analysis of the cracked solar cell samples. (a) Front contact crack-types, (b) Rear contact crack-types

## 145 B. Effect of Breakdown/Micro-Cracks in Solar Cells Fingers

146 Due to the existence of micro cracks, it was observed that out of all examined samples, almost there are  
 147 1500 samples that has a breakdown/cracks in the solar cell fingers, resulting a less forward current  
 148 generation of the solar cell. Two examples of the micro crack, damage and discontinuity in the solar cell  
 149 fingers are shown in Figs. 5(a) and 5(b).

150 There is an increase in the output power loss due to the cracked/damaged fingers. In order to calculate the  
 151 power loss in a single finger, the integration of the length for the finger starting from 0 to L (shown in Fig.  
 152 5(c)) gives the power loss as calculated by (2).

$$153 \quad \text{Power loss} = \int_{x=0}^{x=L} \frac{(x J_{MPP} S_f)^2}{w_f d_f} dx = \frac{1}{3} L^3 J_{MPP}^2 S_f^2 \frac{\rho_f}{w_f d_f} \quad (2)$$

154 where  $L = 2\text{cm}$  is the finger length,  $J_{MPP} = 30\text{ mA/cm}^2$  is the current at maximum power point,  $S_f =$   
 155  $2\text{mm}$  is the finger spacing,  $\rho_f = 1.82 \times 10^{-8}\ \Omega\text{m}$  is the effective resistivity of the metal,  $w_f = 25\ \mu\text{m}$  is  
 156 the finger width, and  $d_f = 13\ \mu\text{m}$  corresponds to the finger depth (or height); all parameters values are  
 157 taken from solar cell manufacturer datasheet.



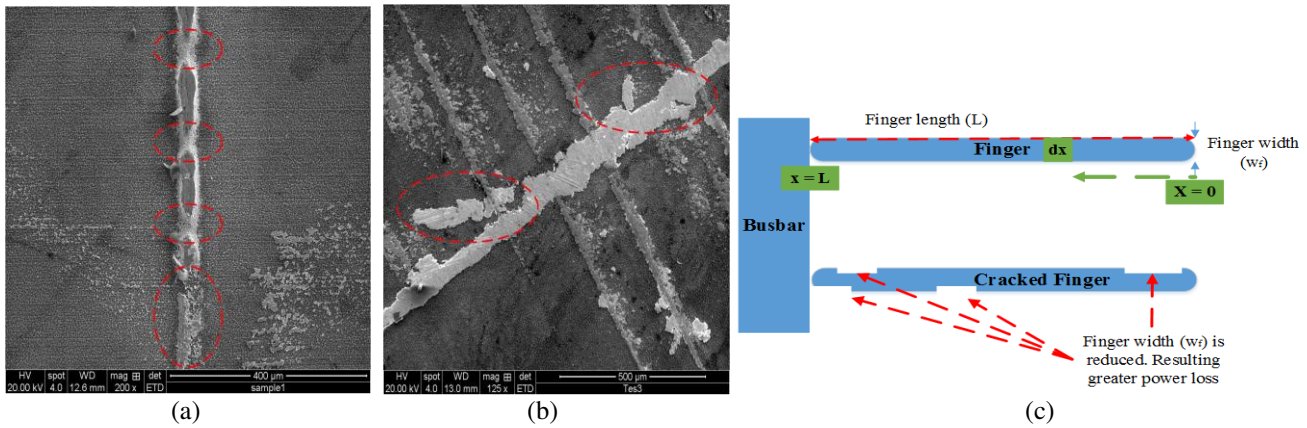


Fig. 5. (a) Cracked – non discontinuity in solar cell finger, sample 1, (b) Cracked – non discontinuity in solar cell finger, sample 2, (c) Illustration on the fingers main parameters, where the width of the cracked finger is reduced resulting a greater power loss

158 As shown in Figs. 7(a) and 7(b), the measured total power loss for the solar cell finger without the existence  
 159 of micro cracks is equal to 3.8%, while it is increased to 5.0% for the cracked finger sample. The main  
 160 reason in the increase of the power loss is due to the decrease in the finger width. Therefore, According to  
 161 (2), if the width of the finger  $w_f$  decrease, the finger power loss will increase. Furthermore, the cracks in  
 162 the solar cell fingers increase the heat-level of the affected solar cell, because the forward current will be  
 163 delivered though marginal size of metal (due to the reduction of the finger width size). Consequently, this  
 164 will create a hot-spot in the finger and will reduce the forward current delivered by the cracked cell. Fig.  
 165 6(a) shows a cracked solar cell sample tested under STC conditions, where two fingers are cracked.

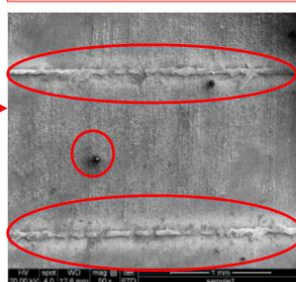
166 The obtained results shown in Fig. 7 are measured using the analysis of a healthy vs. micro cracked solar  
 167 cell sample under STC. The setup of the class AAA LED flasher is shown in Fig. 6(b). The solar cell sample  
 168 has been placed inside the LED-based flasher, whereas a control unit is used to attain a light intensity of  
 169 1000 W/m<sup>2</sup> and ambient temperatures of 25 °C. Thereafter, the output power, current and resistive loss are  
 170 measured using a data acquisition system which uses LabVIEW software. It is also worth noting that all  
 171 tested samples get an illumination of 1000 W/m<sup>2</sup> for a period of 5 milliseconds, this is the fastest rate of  
 172 change that is possible for the flasher to switch its mode from the on/off state. Therefore the observed heat-  
 173 map and thermal-image corresponds to the actual change of the heat across the surface of the solar cell.

**Solar Cell Tested Under STC;**

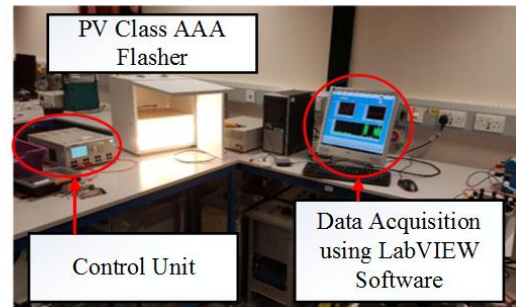
1. Solar irradiance = 1000 W/m<sup>2</sup>
2. Surface Temperature = 25 °C



**Both Fingers are Cracked**



(a)



(b)

Fig. 6. (a) Cracked solar cell tested under STC, (b) PV Class AAA Flasher setup

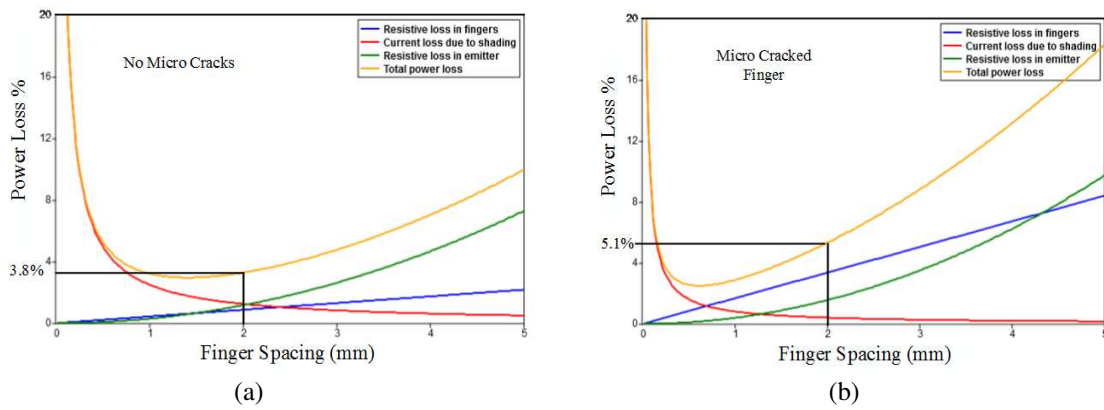


Fig. 7. (a) Power loss estimation (~3.8%) for finger without existence of micro cracks, (b) Power loss estimation (~42%) for finger including micro cracks

174 The output heat-map/thermal-image of the solar cell is shown in Fig. 8. By contrast with the results shown  
 175 in Fig. 8(a), after ten seconds of evaluating the solar cell sample under STC, the temperature of the cracked  
 176 area raised to 72.6 °C, whereas adjacent regions started to heat-up to a limit of 42.5 °C. Interestingly, due  
 177 to the expansion of the heat over the whole solar cell, the heat of the cracked area started to decrease due  
 178 to the flow of the heat over the full cell sample. In Fig. 8(b), thermal image of the solar cell sample is  
 179 captured after 60 seconds, it is evident that the cracked area has a lower temperature of 43.9 °C, but more  
 180 area of the solar cell is affected by a rise in the temperature. In addition, according to Fig. 8(c), after 120  
 181 seconds (the test sample was still under STC), the solar cell sample almost have an identical temperature  
 182 level of 34.3 °C, compared to original temperature of 26.7 °C, therefore, the increase of the solar cell  
 183 temperature due to the existence of the micro cracks is raised by 7.6 °C. It is worth noting that this  
 184 temperature level remains same after 120 seconds. This result confirms that micro cracks in solar cells cause  
 185 hot-spots, where the main heat source of the cell is spread from the original cracked area, and it heats up  
 186 significantly due to the excitation of the electrons through a thinner width of the metal carrying the current  
 187 either in the fingers or busbars, subsequently an increase in the solar cell temperature will be garneted, as  
 188 well as an increase in the output power loss would highly be expected.

189 By contrast with above results, the heat is transferred from the hot-spot area to the rest of the solar cell due  
 190 to the concept of heat by conduction. Conduction is the transfer of heat energy through a solid by the  
 191 collision and vibration of molecules in the solar cell, without movement of the bulk material. For example,  
 192 the hot-spotted area molecules interact with neighboring molecules, transferring some of their energy (heat)  
 193 to these adjacent particles. And since this heat would decrease in the hot-spotted area and increase in the  
 194 adjacent area, the solar cell temperature went steady. This phenomenon is well-known by the transient  
 195 conduction where the heat is not only transferred through the solid using the vibration of the molecules but  
 196 also as a function of time [24].

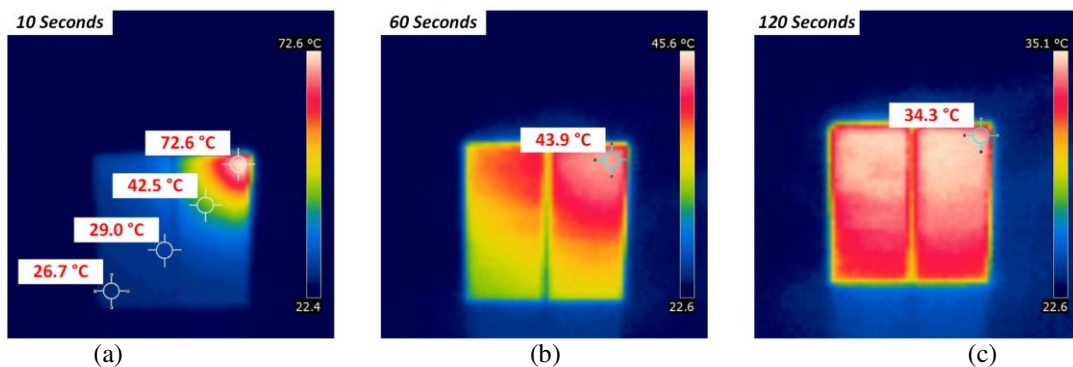


Fig. 8. Heat-Map distribution of the cracked solar cell shown in Fig. 6, operating under STC, images are captured using FLIR thermal camera. (a) After 10 seconds, (b) After 60 seconds, (c) After 120 seconds – this level of temperature remains steady

197 According to [25] it was observed that 78% of the reverse power is turned into heat at the hot-spot area.  
 198 The remaining fraction of the power was evenly distributed over the cell, accounting for the normal reverse  
 199 current, possible contact resistance and additional small shunts. Consequently, the distribution of the heat  
 200 over the cell is generated due to the reverse current flowing from the hot-spotted area throughout the cell  
 201 using the adjacent fingers and busbar, successively reducing the output generated power of the affected  
 202 solar cell. Similarly, authors in [26] presented a new method which provides simple and fast evaluation of  
 203 the hot-spotted solar cells. It was shown that the heat of the affected solar cell by possible hot-spots could  
 204 be distributed across the adjacent locations after a period of 60ms, where the main cause of the heat  
 205 distribution is due to the existence of non-cracked fingers and busbars.

206 In order to determine the I-V and P-V curves of the solar cell sample under STC, an experiment has been  
 207 carried out using the class AAA LED flasher shown in Fig. 6(b). The obtained I-V and P-V curves are  
 208 presented in Fig. 9. Compared to the theoretical predictions (discussed earlier in Table 1), the solar cell  
 209 sample has almost equal  $V_{mpp}$  of 0.48V. However, there is drop in the  $I_{mpp}$  by 0.286A;  $I_{mpp}$  (theoretical:  
 210 6.46A) –  $I_{mpp}$  (cracked solar cell: 6.174A). Resulting an output power loss of 4.39%; calculated as follows:

211 
$$Power\ Loss\ (\%) = 100 - \left( \frac{2.964 (P_{Micro\ cracked\ solar\ cell})}{3.1 (P_{Theoretical\ maximum\ power})} \times 100 \right) = 4.39\%$$

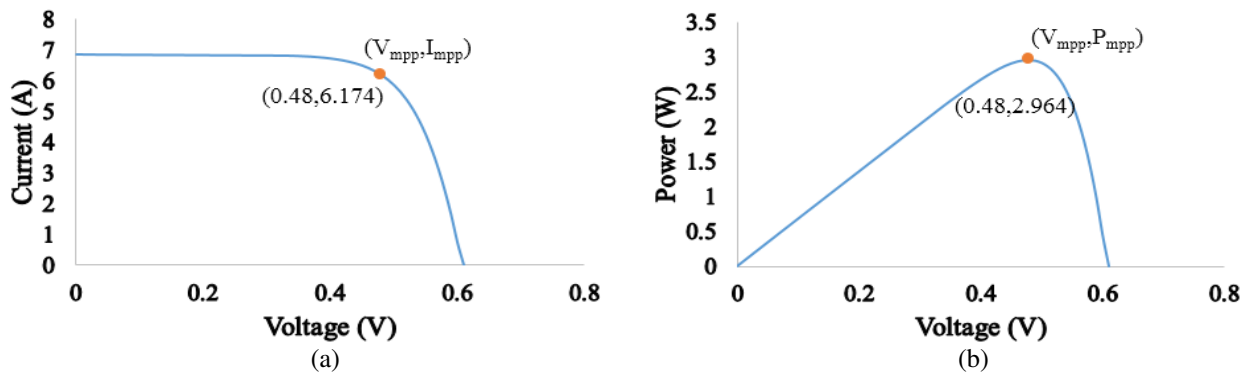


Fig. 9 Obtained I-V & P-V curves of the cracked solar cell sample shown in Fig. 6(a) under STC

212 Another example of cracked fingers has been examined, the cracked cell is shown in Fig. 10. The cell is  
 213 affected by three cracked fingers, where it is evident that there is a discontinuity in the finger connections,  
 214 this would result an increase in the amount of heat generated by this particular case.

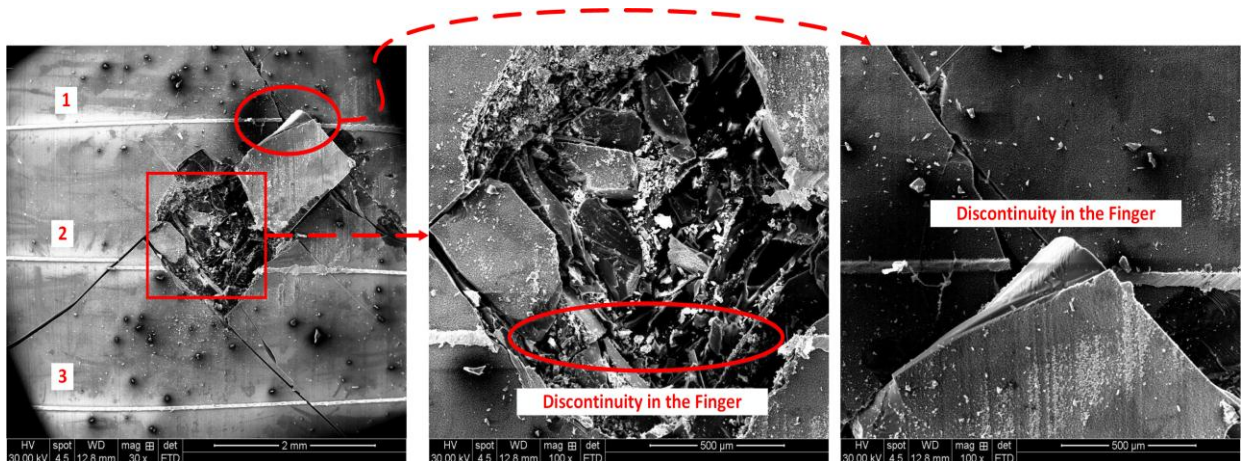


Fig. 10. Micro crack affecting three fingers – there is a discontinuity in the finger connection to the main busbar

215 The examination of the heat-level of the solar cell, starting at 0 second; where the cell has not yet been  
 216 tested under STC, ending up with 100 seconds, where at this stage the cell temperature remains at constant  
 217 level. The results of the experiment are shown in Fig. 11.

218 At zero seconds, the temperature of the cell is equal to 24.3 °C. The temperature of the cracked area raised  
 219 to 105.1 °C after 20 seconds of testing the cell under STC. Ultimately, the heat-level of the cracked would  
 220 decrease, due to the expansion of the heat over the cell, resulting a temperature levels of:

- 221 1) 83.6 °C (40 seconds)
- 222 2) 70.9 °C (60 seconds)
- 223 3) 55.8 °C (80 seconds)
- 224 4) 40.2 °C (100 seconds) - this level of temperature remains consistent

225 In contrast with the results of the heat-distribution, the solar cell had an increase in the temperature of about  
 226 15.9 °C; final temperature level 40.2 °C – original temperature level 24.3 °C. Therefore, this results  
 227 confirms that micro cracks in solar cells are one of the main cause of PV hot-spotting, as well as, the  
 228 increase in the size of cracked area, ultimately will increase the heat-level of the hot-spot in the affected  
 229 solar cell.

230 The solar cell sample has been tested under STC. The obtained I-V and P-V curves are presented in Fig.  
 231 12. Compared to the theoretical predictions (discussed earlier in Table 1), the sample has almost equal  $V_{mpp}$   
 232 of 0.47V. However, there is drop in the  $I_{mpp}$  by 0.662A. Hence, the output power loss is equal to 12.09%;  
 233 calculated as follows:

234 
$$Power\ Loss\ (\%) = 100 - \left( \frac{2.725 (P_{Micro\ cracked\ solar\ cell})}{3.1 (P_{Theoretical\ maximum\ power})} \times 100 \right) = 12.09\%$$

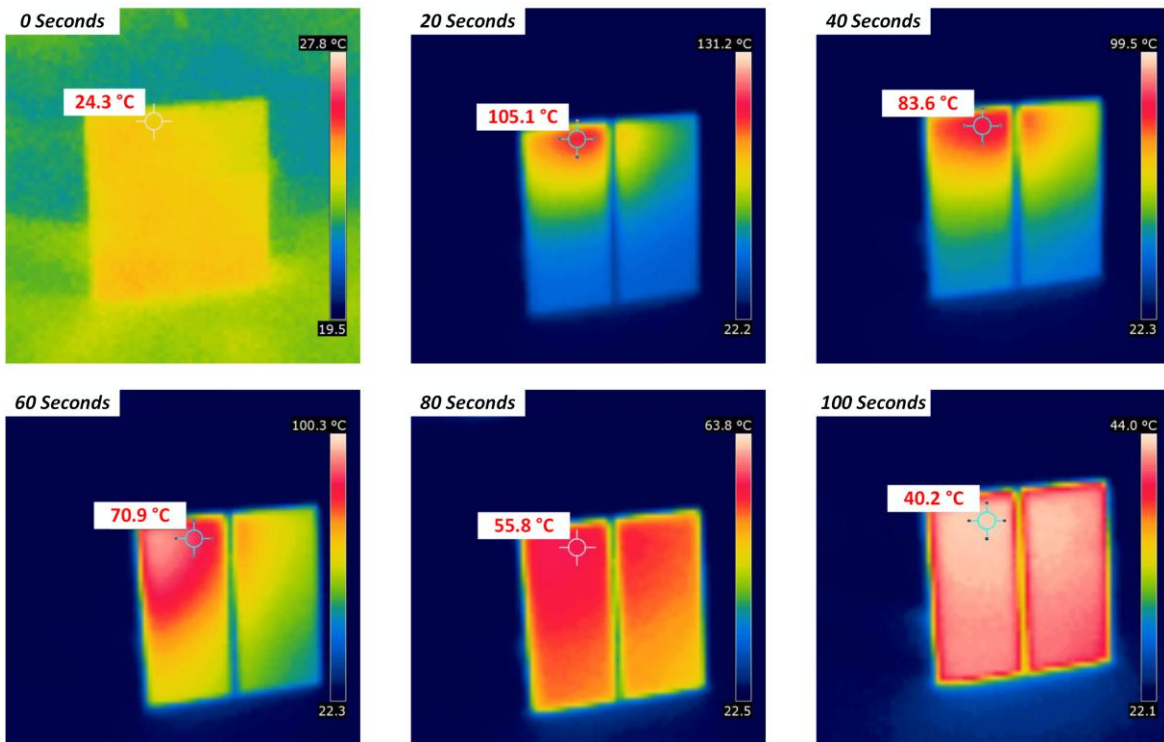


Fig. 11. Heat-Map distribution from 0 to 100 seconds of the cracked solar cell shown in Fig. 9; the solar cell is operated under STC

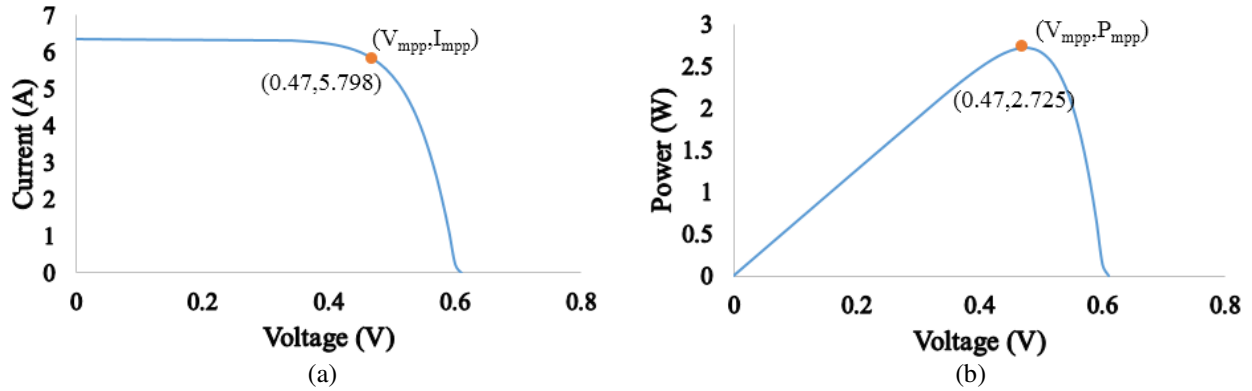


Fig. 12 Obtained I-V & P-V curves of the cracked solar cell sample shown in Fig. 10 under STC

235 **C. Impact of Busbars and Rear Contact Surface Damage due to Micro Cracks and Poor**  
 236 **Manufacturing/Soldering Practice**

237 Due to the Another remarkable result was observed while examining the solar cell samples, out of 4000  
 238 there are 680 affected by cracks in the busbar. The micro cracks in the busbar leads to significant damage  
 239 in the metal driving the current from the fingers outer to an external circuit. On the other hand, almost 380  
 240 solar cell samples are affected by poor soldering.

241 A sample showing a poor adjustment of the busbar metal is shown in Fig. 13. As noticed, there are a number  
 242 of cracks in the solar wafer, while the busbar contains multiple cracks. The silicon (Si) chemical  
 243 composition is present instead of original chemical composition of the silver (Ag). This poor busbar  
 244 structure leads to a second breakdown in the solar cell sample, ultimately causing hot-spot.

245 The solar cell shown in Fig. 13 has been examined under STC (experimental setup similar to Fig 6). The  
 246 solar cell has a micro crack as well as poor soldiering in the busbar. It is expected after 10 seconds the heat  
 247 would increase significantly in the cracked area, and as shown in Fig. 14(a), the temperature of the cracked  
 248 area increased to abnormal level of 91.4 °C. After 60 seconds, the heat started to expand over the entire  
 249 solar cell, where the busbar and the cracked area has a temperature of 77.3 °C, as presented in Fig. 14 (b).

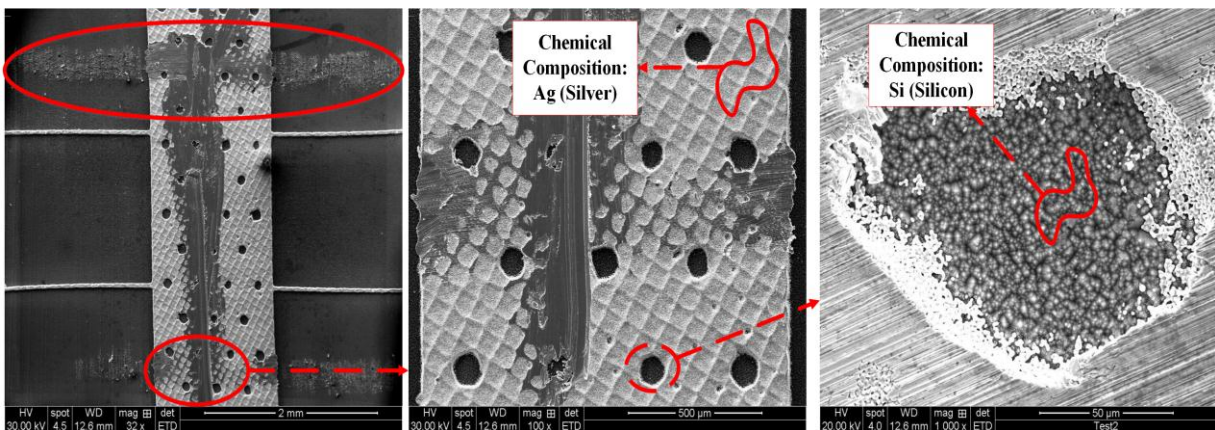


Fig. 13. Micro cracks and soldering mismatch in a solar cell busbar

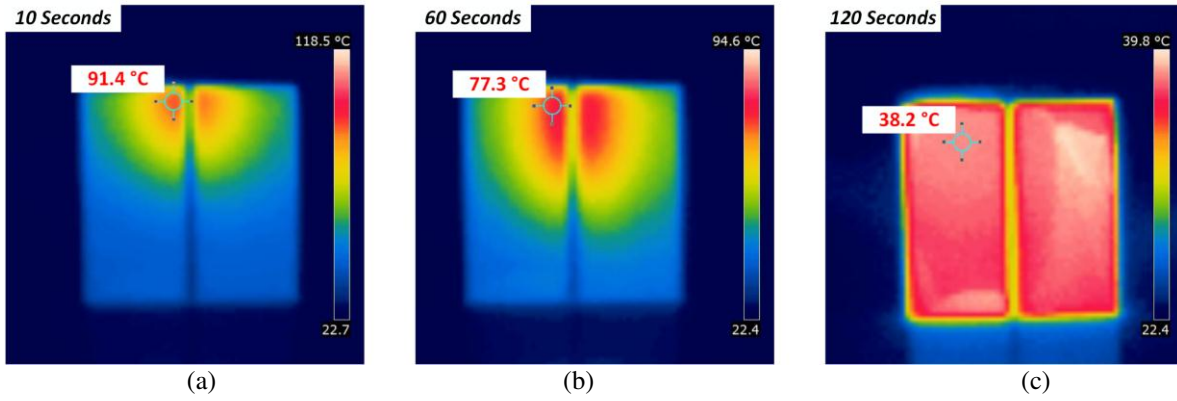


Fig. 14. Heat-Map distribution of the cracked solar cell shown in Fig. 8. (a) After 10 seconds of operating the solar cell under STC, (b) After 60 seconds, (c) After 120 seconds – this level of temperature remains consistent

250 According to Fig. 14(c), the heat is spread all over the solar cell sample, the temperature is equal to 38.2  
 251 °C; this temperature level stays consistent after 120 seconds. Therefore, this experiment proves that cracks  
 252 in solar cell busbars have a significant impact on the solar cell heat level, ultimately initiating hot-spots.

253 I-V and P-V curves for the solar cell sample have been measured under STC, results are presented in Fig.  
 254 15. The measured  $V_{mpp}$  of 0.48V is identical with the theoretical predictions (presented earlier in Table 1).  
 255 However, there is a drop in the maximum output current of 0.15A;  $I_{mpp}$  (theoretical: 6.46A) –  $I_{mpp}$  (cracked  
 256 solar cell: 6.31A). Resulting a loss in the output power equals to 2.19%; calculated as follows:

$$257 \quad \text{Power Loss (\%)} = 100 - \left( \frac{3.032 (P_{\text{Micro cracked solar cell}})}{3.1 (P_{\text{Theoretical maximum power}})} \times 100 \right) = 2.19\%$$

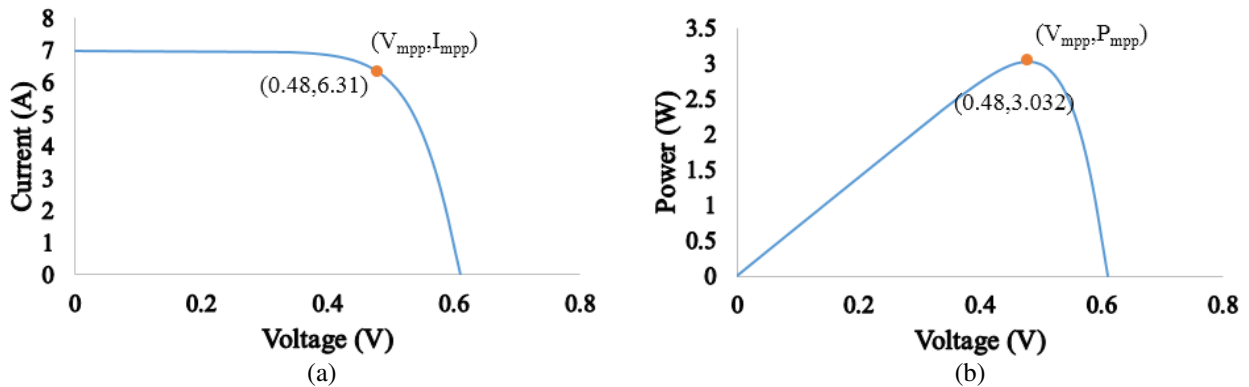


Fig. 15 Obtained I-V & P-V curves of the cracked solar cell sample shown in Fig. 13 under STC

258 The rear contact of a typical solar cell is far less important than the front contact, since it is much further  
 259 away from the junction. However, the design of the rear contact is becoming progressively essential as  
 260 overall efficiency increases and the solar cells become thinner. During the investigation of the rear contact  
 261 of the examined solar cells, it was found that 320 solar cells are cracked; 240 samples are cracked in the  
 262 surface, while 80 samples are cracked in both the surface and the rear busbar. Fig 16 shows the rear  
 263 contact/view of an examined solar cell sample. The difference between the cracked and non-cracked area  
 264 are shown in the figure. Principle, the cracked area consists of two chemical composition of aluminum (Al)  
 265 and silicon (Si), while the non-cracked area is only made of aluminum.

266 As shown in Fig. 16, the non-cracked area has multiple micro cracks of 50  $\mu\text{m}$  width; nevertheless, it does  
 267 not have a noteworthy loss to the solar cell rear contact. However, the actual size of cracked rear area varies  
 268 from 4mm to 300  $\mu\text{m}$ . This damage in the rear contact of solar cell resulting a limited open circuit voltage  
 269 ( $V_{oc}$ ), subsequently will reduce the efficiency of the cell. In light of what was observed during the  
 270 experiments, hot-spotting phenomena has no correlation with the presence of micro cracks in solar cells  
 271 rear contact surface.

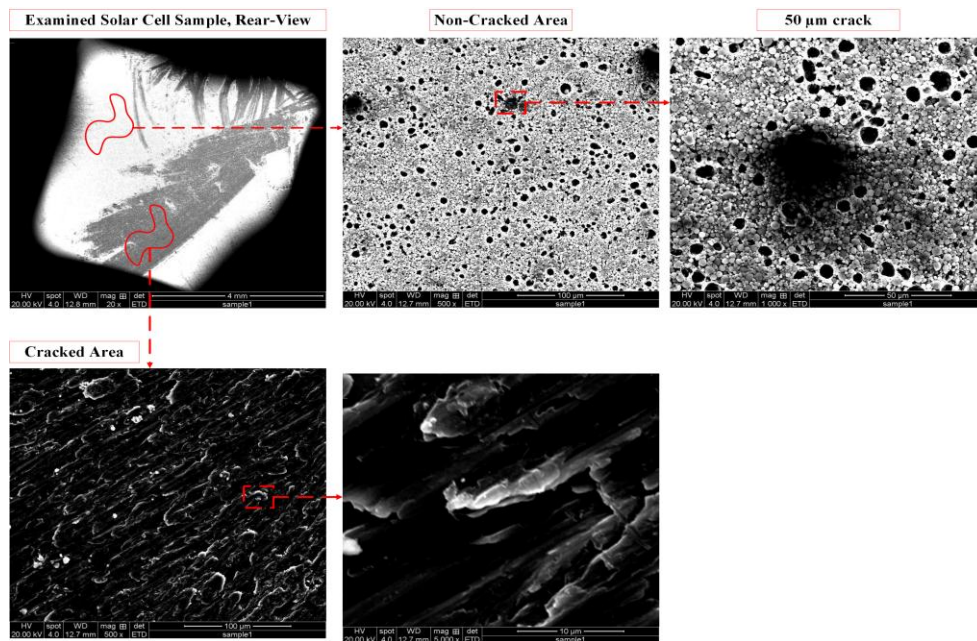
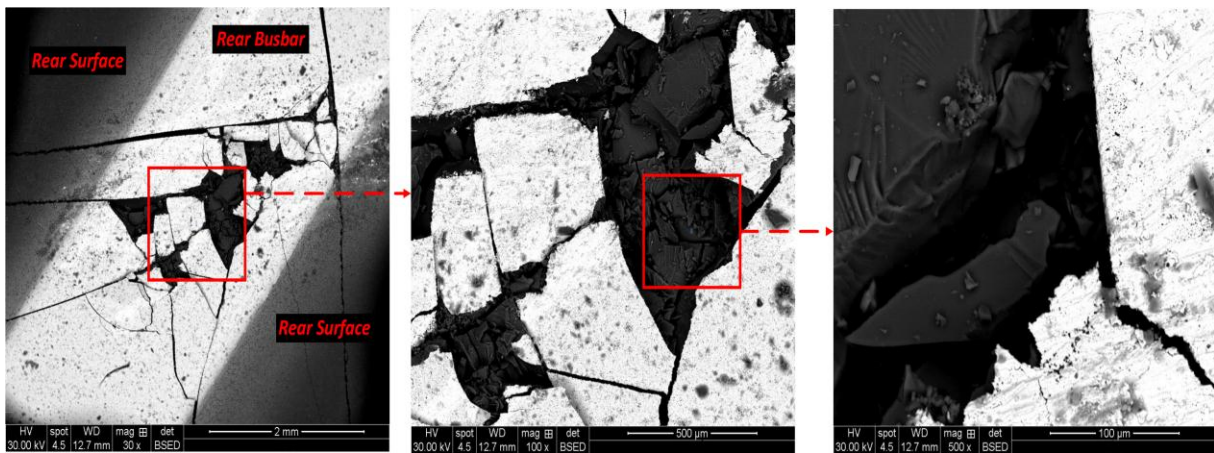


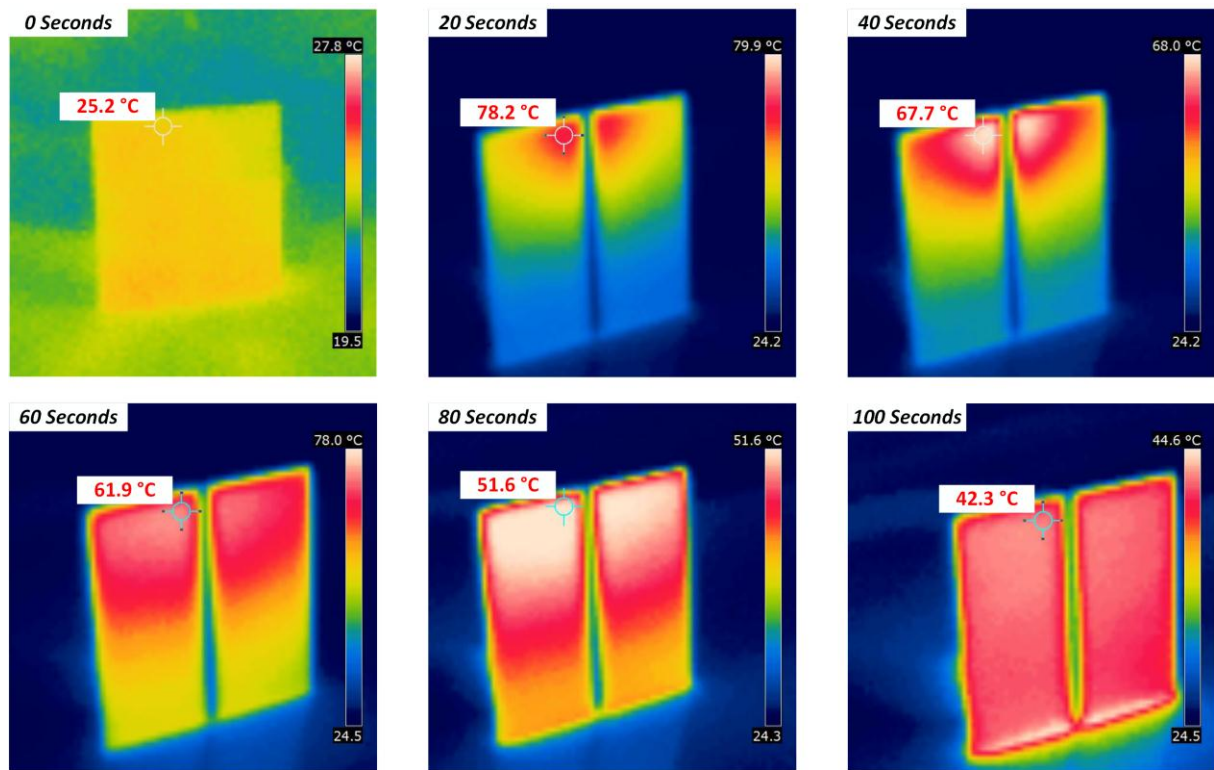
Fig. 16. Micro cracks affecting rear contact of a solar cell

272 Likewise, Fig. 17(a) shows a rear contact image for a solar cell samples affected by micro cracks in the  
 273 surface and busbar. The solar cell was tested under STC, while the temperature of the cell has been captured  
 274 and reported in Fig. 17(b); image is taken from 0 seconds to 100 seconds.

275 At zero seconds, the temperature of the cell is equal to 25.2  $^{\circ}\text{C}$ . The temperature of the cracked area raised  
 276 to 78.2  $^{\circ}\text{C}$  after 20 seconds. Eventually, the heat-level of the cracked area will decrease, due to the expansion  
 277 of the heat over the cell and would result a temperature levels of 67.7  $^{\circ}\text{C}$  (40 seconds); 61.9  $^{\circ}\text{C}$  (60 seconds);  
 278 51.6  $^{\circ}\text{C}$  (80 seconds); and 42.3  $^{\circ}\text{C}$  (100 seconds), this level of temperature remains consistent. In light with  
 279 the results of the heat-distribution, the solar cell had an increase in its temperature of 17.1  $^{\circ}\text{C}$ ; final  
 280 temperature level 42.3  $^{\circ}\text{C}$  – original temperature level 25.2  $^{\circ}\text{C}$ . Therefore, this result shows the impact of  
 281 micro cracks on the rear contract temperature, while it was evident that there is an abnormal increase in the  
 282 cell temperature while performing at STC.



(a)



(b)

Fig. 17. Micro cracks affecting rear contact surface and busbar of a solar cell. (a) Crack affected rear surface and busbar; images magnification of 2mm, 500 $\mu$ m and 100 $\mu$ m, (b) Heat-Map distribution from 0 to 100 while the solar cell is illuminated under STC

283 I-V and P-V curves for the solar cell sample have been measured under STC, results are presented in Fig.  
 284 18. The measured  $V_{mpp}$  of 0.48V is identical with the theoretical predictions (presented earlier in Table 1).  
 285 However, there is a drop in the maximum output current of 0.215A;  $I_{mpp}$  (theoretical: 6.46A) –  $I_{mpp}$  (cracked  
 286 solar cell: 6.245A). Resulting a loss in the output power equals to 3.29%; calculated as follows:

287

$$Power\ Loss\ (\%) = 100 - \left( \frac{2.998 (P_{Micro\ cracked\ solar\ cell})}{3.1 (P_{Theoretical\ maximum\ power})} \times 100 \right) = 3.29\%$$



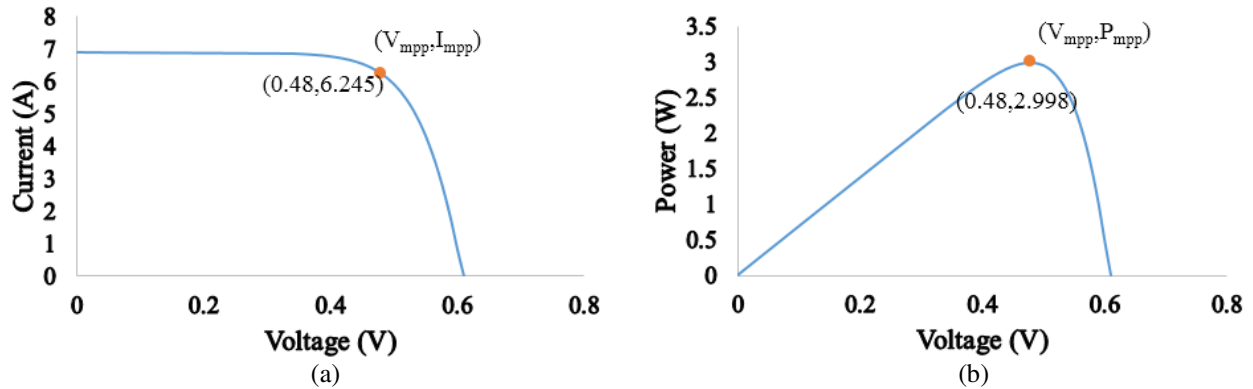


Fig. 18 Obtained I-V & P-V curves of the cracked solar cell sample shown in Fig. 17(a) under STC

#### 288 IV. Conclusion

289 The impact of Photovoltaic (PV) micro cracks has been assessed through the analysis of 4000  
 290 polycrystalline silicon solar cells. The inspection of the cracks has been carried out using an electron  
 291 microscopy, which facilitate the detection of the cracks though the acquisition of both Everhart-Thornley  
 292 Detector (ETD) and the Back Scatted Electron Diffraction (BSED) image, where it was found that the size  
 293 micro cracks are ranging from  $50\mu\text{m}$  to a maximum of 4mm. Micro cracks have been categorized into two  
 294 main categories, including:

- 295 1) Front contact cracks affecting wafer, fingers and busbar.
- 296 2) Rear contact cracks affecting rear furnace and the busbar.

297 Various remarkable observations have been found, including:

- 298 1) The output power loss due to micro cracks ranging from 0.9 to 42.8%.
- 299 2) Cracks in solar cells fingers reduce the finger width, resulting an increase in the power loss by at  
 300 least 1.7%.
- 301 3) There is a significant correlation between PV hot-spots and existence of micro cracks. While the  
 302 temperature of a cracked solar cell sample could increase by  $7.6\text{ }^{\circ}\text{C}$  or more, resulting a permanent  
 303 hot-spots in the affected cell.

304 In future, it is intended to investigate the mitigation of micro cracks in solar cells, and develop a novel  
 305 intelligent detection system to locate and possibly evaluate the impact of such cracks on the output power  
 306 performance of solar cells.

#### 307 V. References

- 308 [1]. IEC 61215:2006, International standard, crystalline silicon terrestrial photovoltaic (PV) modules –  
 309 design qualification and type approval, European committee for Electrotechnical Standardizations.  
 310 Photovoltaic (PV) module safety qualification.
- 311 [2]. Borri, C., Gagliardi, M., & Paggi, M. (2018). Fatigue crack growth in Silicon solar cells and  
 312 hysteretic behaviour of busbars. Solar Energy Materials and Solar Cells, 181, 21-29.  
 313

- 314 [3]. Dhimish, M., Holmes, V., Mather, P., Aissa, C., & Sibley, M. (2018). Development of 3D graph-  
315 based model to examine photovoltaic micro cracks. *Journal of Science: Advanced Materials and*  
316 *Devices*, 3(3), 380-388.
- 317 [4]. Aly, A., Jensen, S. S., & Pedersen, A. B. (2017). Solar power potential of Tanzania: Identifying  
318 CSP and PV hot spots through a GIS multicriteria decision making analysis. *Renewable Energy*,  
319 113, 159-175.
- 320 [5]. Dhimish, M., Holmes, V., Mehrdadi, B., Dales, M., & Mather, P. (2018). Output-power  
321 enhancement for hot spotted polycrystalline photovoltaic solar cells. *IEEE Transactions on Device*  
322 *and Materials Reliability*, 18(1), 37-45.
- 323 [6]. Srečković, N., Lukač, N., Žalik, B., & Štumberger, G. (2016). Determining roof surfaces suitable  
324 for the installation of PV (photovoltaic) systems, based on LiDAR (Light Detection And Ranging)  
325 data, pyranometer measurements, and distribution network configuration. *Energy*, 96, 404-414.
- 326 [7]. Xiang, C., Zhao, X., Tan, L., Ye, J., Wu, S., Zhang, S., & Sun, L. (2019). A solar tube: Efficiently  
327 converting sunlight into electricity and heat. *Nano Energy*, 55, 269-276.
- 328 [8]. El-Bashir, S. M., Al-Harbi, F. F., Elburaih, H., Al-Faifi, F., & Yahia, I. S. (2016). Red  
329 photoluminescent PMMA nanohybrid films for modifying the spectral distribution of solar  
330 radiation inside greenhouses. *Renewable Energy*, 85, 928-938.
- 331 [9]. Bedrich, K. G., Luo, W., Pravettoni, M., Chen, D., Chen, Y., Wang, Z., ... & Wang, Y. (2018).  
332 Quantitative Electroluminescence Imaging Analysis for Performance Estimation of PID-Influenced  
333 PV Modules. *IEEE Journal of Photovoltaics*, 8(5), 1281-1288.
- 334 [10]. Haase, F., Käsewiter, J., Nabavi, S. R., Jansen, E., Rolfes, R., & Köntges, M. (2018). Fracture  
335 Probability, Crack Patterns, and Crack Widths of Multicrystalline Silicon Solar Cells in PV  
336 Modules During Mechanical Loading. *IEEE Journal of Photovoltaics*, 8(6), 1510-1524.
- 337 [11]. Dhimish, M., Holmes, V., Dales, M., & Mehrdadi, B. (2017). Effect of micro cracks on  
338 photovoltaic output power: case study based on real time long term data measurements. *Micro &*  
339 *Nano Letters*, 12(10), 803-807.
- 340 [12]. Oh, S., Jun, D. H., Shin, K. W., Choi, I., Jung, S. H., Choi, J., ... & Yoon, E. (2016). Control of  
341 Crack Formation for the Fabrication of Crack-Free and Self-Isolated High-Efficiency Gallium  
342 Arsenide Photovoltaic Cells on Silicon Substrate. *IEEE Journal of Photovoltaics*, 6(4), 1031-1035.
- 343 [13]. Bressan, M., Gutierrez, A., Gutierrez, L. G., & Alonso, C. (2018). Development of a real-time  
344 hot-spot prevention using an emulator of partially shaded PV systems. *Renewable Energy*, 127,  
345 334-343.
- 346 [14]. Dhimish, M., Holmes, V., Mather, P., & Sibley, M. (2018). Novel hot spot mitigation technique  
347 to enhance photovoltaic solar panels output power performance. *Solar Energy Materials and Solar*  
348 *Cells*, 179, 72-79.
- 349 [15]. Rossi, D., Omaña, M., Giaffreda, D., & Metra, C. (2015). Modeling and detection of hotspot in  
350 shaded photovoltaic cells. *IEEE Transactions on Very Large Scale Integration (VLSI) Systems*,  
351 23(6), 1031-1039.
- 352 [16]. Dhimish, M., Mather, P., & Holmes, V. (2018). Evaluating Power Loss and Performance Ratio of  
353 Hot-Spotted Photovoltaic Modules. *IEEE Transactions on Electron Devices*, 65(12), 5419-5427.
- 354 [17]. S. Ben-Yaakov, A. Cervera, A. Blumenfeld and M. M. Peretz, "Resonant switched-capacitor  
355 gyrator-type converter with local MPPT capability for PV cells". U.S. Patent No. 9,906,189.  
356 Washington, DC: U.S. Patent and Trademark Office, Feb. 2018.

- 357 [18]. Dhimish, M. (2019). Assessing MPPT Techniques on Hot-Spotted and Partially Shaded  
358 Photovoltaic Modules: Comprehensive Review Based on Experimental Data. *IEEE Transactions*  
359 *on Electron Devices*, 66, 1132-1144.
- 360 [19]. Mao, P., Wei, Y., Li, H., & Wang, J. (2017). Junction diodes in organic solar cells. *Nano energy*,  
361 41, 717-730.
- 362 [20]. Bressan, M., Gutierrez, A., Gutierrez, L. G., & Alonso, C. (2018). Development of a real-time  
363 hot-spot prevention using an emulator of partially shaded PV systems. *Renewable Energy*, 127,  
364 334-343.
- 365 [21]. Dhimish, M. (2019). 70% decrease of hot-spotted photovoltaic modules output power loss using  
366 novel MPPT algorithm. *IEEE Transactions on Circuits and Systems II: Express Briefs*.
- 367 [22]. Nolze, G., Winkelmann, A., & Boyle, A. P. (2016). Pattern matching approach to  
368 pseudosymmetry problems in electron backscatter diffraction. *Ultramicroscopy*, 160, 146-154.
- 369 [23]. Zhang, X., Cen, X., Ravichandran, R., Hughes, L. A., & van Benthem, K. (2016). Simultaneous  
370 scanning electron microscope imaging of topographical and chemical contrast using in-lens, in-  
371 column, and everhart–thornley detector systems. *Microscopy and Microanalysis*, 22(3), 565-575.
- 372 [24]. Bharadwaj, P., Karnataki, K., & John, V. (2018, June). Formation of Hotspots on Healthy PV  
373 Modules and Their Effect on Output Performance. In 2018 IEEE 7th World Conference on  
374 Photovoltaic Energy Conversion (WCPEC)(A Joint Conference of 45th IEEE PVSC, 28th PVSEC  
375 & 34th EU PVSEC) (pp. 0676-0680). IEEE.
- 376 [25]. Solheim, H. J., Fjær, H. G., Sørheim, E. A., & Foss, S. E. (2013). Measurement and simulation of  
377 hot spots in solar cells. *Energy Procedia*, 38, 183-189.
- 378 [26]. Geisemeyer, I., Fertig, F., Warta, W., Rein, S., & Schubert, M. C. (2014). Fast Hot Spot  
379 Evaluation. 29th EUPVSEC Amsterdam, 2429-2434.